Colloidal Assembly of Magnetic Nanoparticles and Polyelectrolytes by Arrested Electrostatic Interaction

Article *in* Colloids and Surfaces A Physicochemical and Engineering Aspects · November 2016

DOI: 10.1016/j.colsurfa.2016.11.049

CITATIONS
0

READS
106

10 authors, including:

Kun Xiong
Southwest University of Science and Technology
17 PUBLICATIONS **102** CITATIONS
SEE PROFILE

Yong Ren
Southwest University of Science and Technology
34 PUBLICATIONS **349** CITATIONS
SEE PROFILE

Jérémie Courtois
Southwest University of Science and Technology
18 PUBLICATIONS **320** CITATIONS
SEE PROFILE

Minhao Yan
Southwest University of Science and Technology
46 PUBLICATIONS **357** CITATIONS
SEE PROFILE

Some of the authors of this publication are also working on these related projects:

1) Artificial or functionalized natural materials for hazardous/nuclear waste treatment and disposal. 2) Fundamental understanding on colloidal behavior of actinide and geological clays. 3) Supramolecular assembly of lanthanide/actinide system. View project

Nanoparticles for Actinides separation View project

Colloids and Surfaces A: Physicochem. Eng. Aspects 514 (2017) 107–116

Contents lists available at ScienceDirect

Colloids and Surfaces A: Physicochemical and Engineering Aspects

journal homepage: www.elsevier.com/locate/colsurfa

Colloidal assembly of magnetic nanoparticles and polyelectrolytes by arrested electrostatic interaction

Huailiang Li[a,b,1], Mark Julian Henderson[a,c,1], Kunzhou Wang[a], Xianguo Tuo[b], Yangchun Leng[b,c], Kun Xiong[a], Yuliang Liu[a], Yong Ren[a], Jérémie Courtois[a,*], Minhao Yan[a,c,*]

[a] State Key Laboratory Cultivation Base for Nonmetal Composites and Functional Materials, Southwest University of Science and Technology, Mianyang 621010, China
[b] Sichuan University of Science and Engineering, Zigong 643000, China
[c] Fundamental Science on Nuclear Wastes and Environmental Safety Laboratory, Southwest University of Science and Technology, Mianyang 621010, China

HIGHLIGHTS

- Direct mixing of oppositely charged nanoparticles and polymers in solutions.
- Kinetics of self-assembly is decreased and controlled aggregates are generated.
- Simple assembly route can be generally extended for practical applications.

GRAPHICAL ABSTRACT

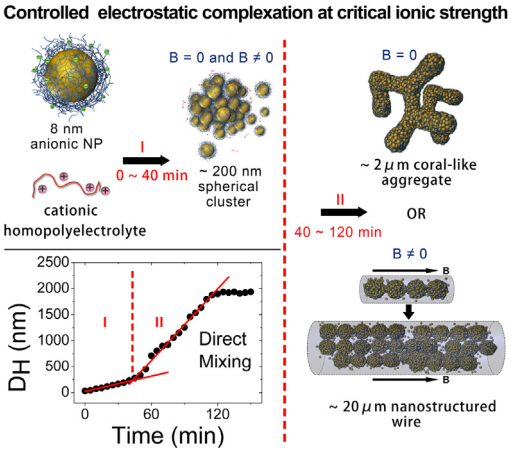

This work presents a simple approach which can efficiently moderate the wild electrostatic attractions between anionic nanoparticles and cationic homopolyelectrolytes. Sizes and morphologies of the synthesized aggregates do not show any dependency on the formulation in terms of charges ratios or on the chemical nature of the polycations. This simple direct mixing process does not require a specific manipulation device which is of great interest for potential applications.

ARTICLE INFO

Article history:
Received 4 August 2016
Received in revised form 20 October 2016
Accepted 22 November 2016
Available online 23 November 2016

Keywords:
Magnetic nanoparticles

ABSTRACT

Electrostatic interaction of charged colloids and polyelectrolytes is a useful method to assemble matter into hybrid nanostructures with numerous examples in materials science as well as in biology. However, the colloidal electrostatic interaction is rapid and uncontrolled, the strong interaction usually leads to large and irregular aggregates. Therefore, control of the electrostatic interaction in order to resulting well-defined nanostructures remains a challenge. Here we report on a general and simple method to moderate the wild electrostatic interaction. Direct mixing of stock solutions containing anionic superparamagnetic nanoparticles and widespread cationic homopolyelectrolytes at an appropriate ionic strength

* Corresponding authors at: State Key Laboratory Cultivation Base for Nonmetal Composites and Functional Materials, Southwest University of Science and Technology, Mianyang 621010, China
E-mail addresses: jeremiecourtois@swust.edu.cn (J. Courtois), yanminhao@swust.edu.cn (M. Yan).
[1] H. L and M. J. H contributed equally to this work.

http://dx.doi.org/10.1016/j.colsurfa.2016.11.049

Polyelectrolytes
Electrostatic interaction
Controllable assembly
Nanostructured wires

generates aggregates with controlled shape and morphology. The simple and versatile methodology not only efficiently moderates electrostatic interactions but also enables the corresponding growth mechanism to be revealed by light scattering and electron microscopy as aggregation occurs at much slower timescales. The present results carry important implications for both practical applications and understanding on nanoscale electrostatic interaction between colloids.

1. Introduction

Although the synthesis of various inorganic nanoparticles (NPs) has been well-established, their controlled assembly into larger superstructures [1–7] remains an ongoing challenge [8,9], en route to applications ranging from medical therapeutics [10,11] and diagnostics [11–14] to photonics [15] and photovoltaics [16,17]. For instance, the establishment of a useful and controllable methodology for the assembly of NPs into well-defined rods or arrays is particularly important because it offers immense opportunities for applications in optoelectronics [18–20] and sensing [21,22]. During the last decade several research groups have reported on the assembly of colloidal particles [23–29]. In spite of the development based on these advanced approaches, the establishment of simple and cost-efficient methodologies for the controllable assembly of NPs into well-defined rods or wires remains a challenge.

Recently electrostatic interactions have been increasingly exploited as a simple and versatile route to assemble NPs into well-defined superstructures with oppositely charged polyelectrolytes (PEs) [30,31]. The process performed at room temperature and atmospheric pressure displays much higher yield than the "grafting-from" or "grafting-to" covalent reactions allowing scaling up any process to large quantities and workloads, as required by industry. The electrostatically driven assembly between PEs and oppositely charged colloids is spontaneous and the direct mixing of their solutions can result in phase separation. This is the case for PEs and surfactants for which micellar coacervates and liquid crystalline phases have been observed [32–34]. Interaction is favored by the electroneutrality of the PE/micelle complex and can be enhanced or suppressed by changing salt concentration as it increases or decreases the binding affinity of micelles to polyelectrolytes [35,36].

In order to control the electrostatic interaction and to preserve the colloidal stability with desired size and shape, a novel mixing protocol for assembling anionic poly(acrylic acid) coated maghemite (γ-Fe_2O_3-PAA) NPs and cationic PEs was recently reported [37–40]. This protocol denoted "desalting kinetic" was inspired by molecular biology techniques developed for the *in vitro* reconstitution of chromatin [41]. Using NPs (γ-Fe_2O_3-PAA) and oppositely charged homopolyelectrolytes (homoPEs) such as poly(diallyldimethylammonium chloride) (PDADMAC) or poly(ethyleneimine) (PEI), this method generates rod-like clusters with regular cylindrical form, but only when one of the oppositely charged species is introduced in large excess [37,39]. The "desalting kinetic" method applied to a mixture of NPs and homoPEs at the isoelectric point (IP)—where the amount of negative charges brought by the NPs equals the amount of positive charges brought by the PEs chains—fails to form regular rod-like clusters but rather creates large and irregular aggregates with macroscopic phase separation [37,39]. Consequently, a general and simpler method that overcomes the restrictive assembly conditions is required.

In this work, we present a useful approach which can efficiently moderate electrostatic attraction during the entire self-assembly. Stock solutions of NPs (γ-Fe_2O_3-PAA) and homoPEs (PDADMAC or PEI) are directly mixed at an appropriate ionic strength I_s of the aqueous medium. In this case, the interaction process is slowed down to the timescale of hours rather than the quasi-spontaneous assembly of existing methods. The increased time of reaction allows aggregation of reactive species into well-defined colloids and also enables the corresponding growth mechanism to be revealed. Using this approach the conditions of assembly, namely the chemical nature of building blocks and assembly protocols are subject to the minimum restrictions.

2. Experimental section

2.1. Materials

The following chemicals were used for synthesis of polymer-coated NPs: $FeCl_2$, H_2O; $FeCl_3$ 27 wt.% in water, hydrochloric acid, sodium hydroxide, ammonia at 20 wt.% in water, nitric acid at 52 wt.% in water, $Fe(NO_3)_3$, acetone, diethyl ether, poly(acrylic acid) (Mw = 2000 g mol^{-1}, polydispersity = 1.7).

Cationic homoPEs included poly(diallyldimethylammonium chloride) (PDADMAC), Mw < 100,000, 35 wt.% in H_2O and poly(ethyleneimine) (PEI), Mw = 2000, 50 wt.% in H_2O. The molecular structures of the cationic homoPEs are shown in Scheme 1.

All chemicals were obtained from Sigma Aldrich and used as received. All the water used in the study was MilliQ quality water (Millipore®).

2.2. Poly(acrylic acid) coated maghemite NPs

2.2.1. Synthesis

Poly(acrylic acid) coated iron oxide NPs were prepared following reported protocols. First, maghemite (γ-Fe_2O_3) nanocrystals were synthesized by the Massart method [42]. Briefly, iron (II) and iron (III) salts are co-precipitated in an alkaline medium at room temperature. The obtained magnetite (Fe_3O_4) nanocrystals were then transferred in nitric acid and oxidized into maghemite by the addition of $Fe(NO_3)_3$ at boiling temperature for 30 min. Their color progressively changed from black to orange-red. Polydispersity of the sample was reduced by size sorting. After two successive liquid-liquid phase separations induced by the addition of large amount of nitric acid [43], γ-Fe_2O_3 nanocrystals of a median diameter of 9.3 nm and a narrow polydispersity of 0.18 were obtained. The bare γ-Fe_2O_3 NPs are positively charged with zeta potential of +30 mV at pH = 2 and T = 25 °C. In these conditions, the net positive charge around the particle surface ensures their reliable colloidal stability [44]. Second, the bare NPs were coated in acidic condition with poly(acrylic acid) oligomers with a molecular weight of 2000 g mol^{-1} using the precipitation-redispersion process [45]. The drop-by-drop addition of a solution of poly(acrylic acid) (PAA_{2K}) at pH = 2 (HNO_3) to a dispersion of bare NPs at pH = 2 (HNO_3) leads to precipitation of the nanocrystals and their adsorbed PAA_{2K} chains. Single particles are then recovered by redispersion at pH = 12 (NH_4OH). The dispersion of PAA_{2K} coated NPs (γ-Fe_2O_3-PAA_{2K}) is finally purified by dialysis in deionized water.

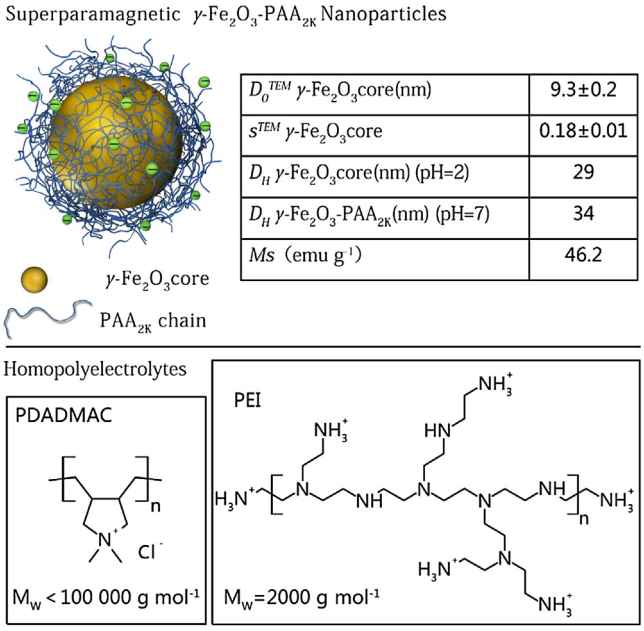

D_0^{TEM} γ-Fe_2O_3core(nm)	9.3±0.2
s^{TEM} γ-Fe_2O_3core	0.18±0.01
D_H γ-Fe_2O_3core(nm) (pH=2)	29
D_H γ-Fe_2O_3-PAA_{2K}(nm) (pH=7)	34
Ms (emu g^{-1})	46.2

Scheme 1. Top: Schematic representation of the superparamagnetic maghemite NPs coated with poly(acrylic acid) oligomers of M_W = 2000 g mol^{-1} (γ-Fe_2O_3-PAA_{2K}) and their physical properties. Terms D_0^{TEM} and s^{TEM} are the median diameter and the polydispersity of the uncoated particles extracted from TEM images analysis, respectively. The D_H γ-Fe_2O_3 core and D_H γ-Fe_2O_3-PAA_{2K} are the hydrodynamic diameters (D_H) measured by Dynamic Light Scattering at T = 25 °C of respectively bare NPs dispersed in water at pH = 2 (HNO_3) and PAA_{2K} coated NPs dispersed in DI water (pH = 7). M_S is the saturation magnetization measured by Vibrating Sample Magnetometry at T = 25 °C. Bottom: Molecular structures and average molecular weight of the two cationic homoPEs of the study: poly(diallyldimethylammonium chloride) (PDADMAC) and poly(ethyleneimine) (PEI).

2.2.2. Characterization

Size and polydispersity of the bare γ-Fe_2O_3 nanocrystals were characterized by TEM. The physical median diameter $D_0^{TEM} = 9.35 \pm 0.2$ nm and polydispersity $s^{TEM} = 0.18 \pm 0.01$ was determined by measuring physical diameters and fitting the distribution in diameters with a log-normal function. A representative TEM image of the NPs, their probability distribution functions of size and its log-normal fitting are presented in the Electronic Supplementary information (ESI) (ESI–1.1). The crystalline structure of the maghemite nanoparticles is revealed by Electron Diffraction Spectroscopy. The diffraction pattern is presented in ESI–1.2. The observed change in color of the dispersion from black to orange-red also gives an indication of oxidation of magnetite to maghemite [46]. The average molecular weight of the γ-Fe_2O_3 NPs was calculated to be 5.82×10^6 g. mol^{-1} by static light scattering (SLS). Experimental details are presented in ESI–1.3.

The hydrodynamic diameter (D_H) found for γ-Fe_2O_3-PAA_{2K} dispersions (pH = 7 and T = 25 °C) is 34 nm which is larger than that of the bare particles (29 nm) indicating the presence of PAA_{2K} brush surrounding the particles (see ESI–1.3).

As reported by a recent publication [47], γ-Fe_2O_3-PAA_{2K} NPs exhibit a negative electrophoretic mobility $\mu_E = -3.6 \pm 0.2$ cm^2 V^{-1} s^{-1} (corresponding to a zeta potential $\zeta_p \sim -48$ mV) at pH = 7, T = 25 °C and without added salt, due to the negative charges of the carboxylate groups at their surface [48]. In this work, γ-Fe_2O_3-PAA_{2K} NPs are mixed with PDADMAC and PEI at 25 °C, pH = 7 and at respectively salt solution [NH_4Cl] = 0.49 M and [NH_4Cl] = 2.6 M. Zeta potentials of NPs dispersion in these conditions were measured by Brookhaven Instruments NanoBrook Omni zeta potential analyzer (shown in Table 1).

Following the acid-base titration presented in ESI–1.4.3, the surface charge density of the γ-Fe_2O_3-PAA_{2K} NPs at pH = 7, T = 25 °C at [NH_4Cl] = 0.49 M and [NH_4Cl] = 2.6 M are respectively 3710 ± 80 and 5370 ± 80 negative charges per nanoparticle.

Table 1
Zeta potentials of γ-Fe_2O_3-PAA_{2K} NPs measured in different concentration of salt solutions at pH = 7 and 25 °C.

Building Blocks	Zeta potential at pH = 7 and 25 °C
γ-Fe_2O_3-PAA_{2K} in 0.49 M NaCl	−22.47 mV
γ-Fe_2O_3-PAA_{2K} in 2.65 M NaCl	−25.28 mV

Vibrating sample magnetometry (VSM) measurements of a liquid dispersion of γ-Fe_2O_3-PAA_{2K} reveals their superparamagnetic behavior at T = 25 °C with saturation magnetization of 46.2 emu g^{-1}. The fitting of the magnetization curve using the Langevin function for superparamagnetism convoluted with a log-normal distribution function of the particle size gives a median diameter D_0^{VSM} that corresponds to the domain of the iron oxide core with a superparamagnetic behavior. The $D_0^{VSM} = 8.3 \pm 0.1$ nm and the polydispersity $s^{VSM} = 0.26 \pm 0.02$; this was calculated for the γ-Fe_2O_3-PAA_{2K} sample. The magnetization curve and Langevin fit are presented in the ESI–1.5. Scheme 1 offers a representation of the superparamagnetic γ-Fe_2O_3-PAA_{2K} NPs and resumes their basic physical properties.

2.3. Direct mixing protocol

In this study, aggregates of NPs and homoPEs were made by direct mixing of stock solutions of the two oppositely charged species at room temperature. Rapid homogenization of the mixture is ensured by repeated drawing/release of the liquid into/out of a pipette.

We prepared a water-based γ-Fe_2O_3-PAA_{2K} NPs dispersion, PDADMAC stock solution, and PEI stock solution at pH = 7 with concentrations of c = 0.5 wt.%, c = 0.05 wt.% and c = 0.005 wt.%, respectively. The NPs and homoPEs solutions at the same concentration are then mixed at a volume ratio of $V_{NP}/V_{poly} = 3.58$ for NPs and PDADMAC mixtures and $V_{NP}/V_{poly} = 3.93$ for NPs and PEI mixtures. The calculation is detailed in ESI–2.1.

Zeta potentials of polyelectrolytes were measured using Brookhaven Instruments NanoBrook Omni zeta potential analyzer. ξ_p of PDADMAC at c = 0.26 wt.%, pH = 7, T = 25 °C and [NH_4Cl] = 0.49 M is +18.47 mV and ξ_p of PEI at c = 0.26 wt.%, pH = 7, T = 25 °C and [NH_4Cl] = 2.6 M is +16.17 mV. The charge densities of PDADMAC and PEI solutions used to prepare the NPs/PE mixtures were determined by acid-base titrations (ESI 1.4.1 and ESI 1.4.2).

The I_s of NPs and homoPEs stock solutions are monitored by the addition of ammonium chloride (NH_4Cl). The I_s of the samples was calculated only considering the contribution of added NH_4^+ and Cl^- via [49]:

$$I_S = \frac{1}{2}\sum_i c_i z_i^2 \quad (1)$$

where c_i and z_i denote the concentration and valency of the ionic atomic species in solution, respectively. The I_s of a given mixture is the consequence of the mixing of two stock solutions of the same I_s.

This work focuses on the moderation of electrostatic interaction by reacting oppositely charged species at a critical value of the ionic strength (I_s^c). Above this critical value, electrostatic interactions are screened and oppositely charged species do not react [37–40]; interaction occurs below the I_s^c. To determine the I_s^c of NPs + PDADMAC and NPs + PEI mixtures, a collection of samples of these respective systems have been prepared by gradually decreasing the I_s by adding an increasing amount of deionized water. For each sample, the hydrodynamic size of the diffusing species was

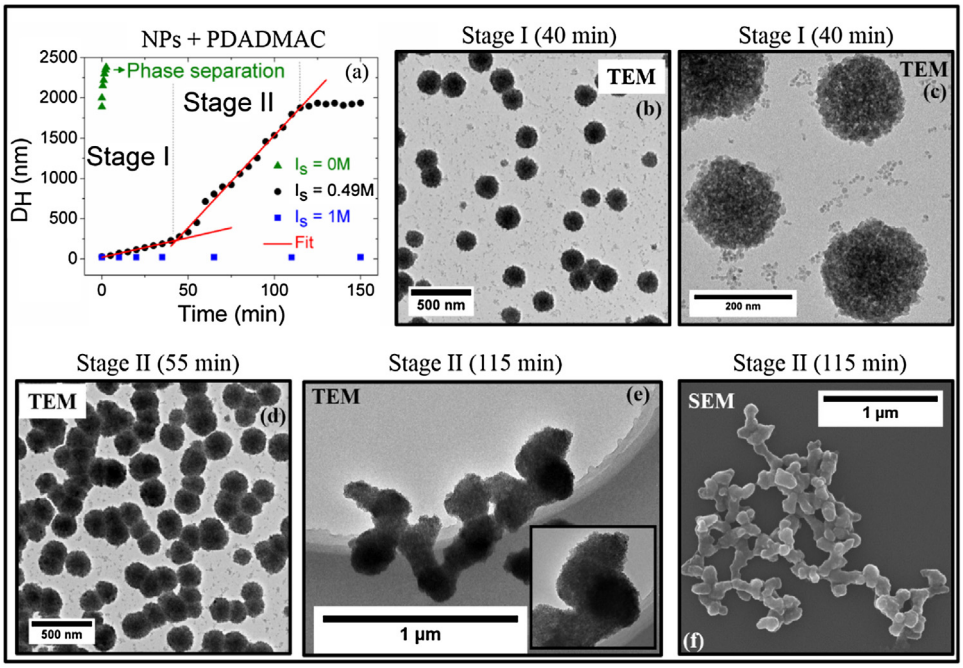

Fig. 1. (a) Hydrodynamic diameter (D_H) versus time of direct mixings of γ-Fe_2O_3-PAA_{2K} NPs dispersion and PDADMAC solutions at c = 0.05 wt.% and at three different I_s. No aggregation is observed when $I_s \gg I_s^c$ (critical ionic strength), spontaneous precipitation occurs at I_s = 0 M, and slow aggregation occurs at $I_s = I_s^c$ with a two-stage growth mechanism. (b, c) TEM images of the spherical aggregates obtained during stage I, 40 min after direct mixing. (d) TEM image of clusters of spherical aggregates obtained at the beginning of stage II (55 min). (e) TEM and (f) SEM images of the coral-like aggregates obtained at the end of stage II (115 min). The insert to (e) shows a zoom-in region of the extremity of an aggregate to display the tightly bound individual particles.

measured via dynamic light scattering (DLS) immediately after mixing. Aggregation between NPs and homoPEs occurs at I_s < 0.5 M for NPs + PDADMAC mixtures and I_s < 2.65 M for NPs + PEI mixtures. Experimental data are presented in ESI–2.2. Consequently, the critical values of the ionic strength I_s^c(NPs + PDADMAC) = 0.49 M and I_s^c(NPs + PEI) = 2.60 M have been chosen for the study of the moderated interaction of NPs and homoPEs. In an initial trial, direct mixtures of NPs + PDADMAC and NPs + PEI at their respective I_s^c are studied by light scattering and electron microscopy. The second trial of experiments repeated the above NPs and homoPEs direct mixing protocol inside a static external 0.3 T magnetic field provided by a permanent magnet.

The synthesized aggregates were concentrated using a permanent magnet and the supernatant removed and replaced by deionized water three times.

In order to obtain aggregates of controlled shape and size, reactions were stopped at the corresponding time by the addition of concentrated sodium chloride solution as the value of I_s became 1 M for NPs + PDADMAC mixtures and 3 M for NPs + PEI mixtures. The obtained aggregates are concentrated using permanent magnet and then washed three times with salty solution at the same concentrated to remove the excess of unreacted building blocks. Afterwards, excess of salt is removed by washing three times with pure water. Finally, aggregates were kept in DI water for the further characterization.

2.4. Characterization of the NPs/homoPEs interaction

2.4.1. Light scattering experiments

Dynamic light scattering was monitored on a Brookhaven 90plus to measure the Rayleigh ratio $R(q,c)$ and the collective diffusion constant $D(c)$. The Rayleigh ratio was obtained from the scattered intensity $I(q,c)$ measured at the wave-vector q according to [50]:

$$R(q,c) = R_{std}\frac{I(q,c) - I_{Water}}{I_{Tol}}\left(\frac{n}{n_{Tol}}\right)^2 \quad (2)$$

R and n_{Tol} are the standard Rayleigh ratio and refractive index of toluene and I_{Water} and I_{Tol} are the intensities measured for the solvent and for the toluene in the same scattering configuration; $q = (4\pi n/\lambda)\sin(\theta/2)$ (n being the refractive index of the solution, θ the scattering angle and λ the wavelength of laser). The scattering angle was $\theta = 90°$ and corresponds to wave-vector $q = 1.87 \times 10^{-3}$ Å^{-1}. In quasi-elastic light scattering, the collective diffusion coefficient D_0 was measured in the dilute concentration range (c = 0.05 wt.%, pH = 7 and 25 °C) with an optimal intensity of $\sim 2 \times 10^5$ counts/s. The hydrodynamic diameter of the colloids was calculated according to the Stokes-Einstein relation, $D_H = k_BT/3\pi\eta D_0$, where k_B is the Boltzmann constant, T the temperature (T = 298 K), and η the solvent viscosity (0.89×10^{-3} Pa. s). The autocorrelation functions of the scattered light were interpreted using both the method of cumulants and the CONTIN fitting procedure provided by the instrument software.

2.4.2. Electron microscopy

Transmission electron microscopy (TEM) and scanning electron microscopy (SEM) were carried out on a Zeiss Libra200FE microscope and Zeiss Ultra55 microscope, respectively, at the Analysis and Characterization Center of Southwest University of Science and Technology.

2.4.3. Optical microscopy

Images of the magnetic wires were acquired on a BX51 microscope (Olympus) equipped with 10 × and 20× objectives. The 2 μL of dispersion at a concentration of 0.01 wt.% were deposited on a glass plate and sealed into a gene frame (Abgene/Advanced Biotech)

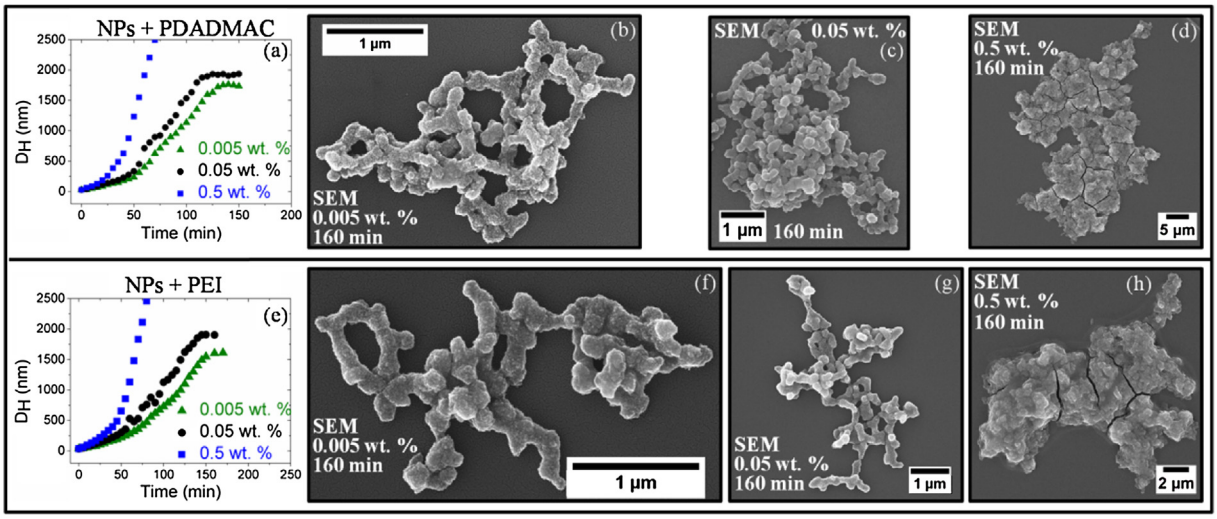

Fig. 2. (a, e) Hydrodynamic diameter (D_H) versus time of direct mixing of γ-Fe_2O_3-PAA_{2K} NPs dispersions and PDADMAC (upper panel) solutions or PEI (lower panel) solutions at 0.5 wt.%, 0.05 wt.% and 0.005 wt.%. For both systems, at all concentrations, direct mixing was performed at I_s^c (0.49 M for NPs + PDADMAC, and 2.60 M for NPs + PEI). SEM images of the aggregates obtained 160 min after direct mixing at 0.005 wt.%. (b, f), at 0.05 wt.%. (c, g) and at 0.5 wt.% (d, h).

dual adhesive system. To determine the length distribution of the wires, pictures were digitized and studied with ImageJ software (http://rsbweb.nih.gov/ij/).

3. Results and discussion

The γ-Fe_2O_3-PAA_{2K} NPs dispersions are directly mixed with PDADMAC or PEI solutions (particles dispersion and polymer solutions with pH = 7 and concentrations of 0.05 wt.%) at IP (see Experimental section) and at three different I_s values: I_s = 0 M, $I_s = I_s^c$ (0.49 M for NPs + PDADMAC, and 2.60 M for NPs + PEI) and $I_s \gg I_s^c$ (1 M for NPs + PDADMAC, and 3 M for NPs + PEI). Fig. 1 presents the DLS measurements of the NPs + PDADMAC mixtures, and TEM and SEM images of aggregates obtained at different time for the mixture made at I_s^c. The results indicate that the mixtures of NPs with either PDADMAC or PEI are similar. The DLS study, TEM and SEM images related to NPs + PEI mixtures are presented in ESI–2.3.

Fig. 1(a) and Fig. S9(a) display respectively the time evolutions of respectively NPs + PDADMAC and NPs + PEI mixtures monitored by DLS. As a consequence of the strong electrostatic interactions, direct mixtures of NPs and PDADMAC or PEI at I_s = 0 M provides an instantaneous phase separation with large aggregates (D_H >2.5 μm). For the mixture at $I_s \gg I_s^c$, the mixed solutions remain clear and homogenous with a constant value of the D_H of 34 nm corresponding to the value of single NPs. Electrostatic interaction does not occur at these high I_s due to charge screening [37,38,40]. In the case of NPs + PEI mixture, very high I_s (3 M) is required to screen their interaction compare with NPs + PDADMAC mixture. One can consider that there may exists not only electrostatic interaction but probably other forces such hydrogen bonding and/or hydrophobic interaction involved. In particular, $-NH_3^+$ from PEI and $-COO^-$ from carboxylated particles are supposed to be able to form a salt bridges, which is a combination of electrostatic interaction and Hydrogen bond, and which is known to be involved in stability of proteins [51]. PEI chains, kept close to each other in NP/PEI aggregates, may also generate attractive forces rising from hydrophobic interaction and Hydrogen bonding [52].

For mixtures at I_s^c, the interaction is effectively moderated versus the mixture at I_s = 0 M with only slow aggregation. Aggregation can be described by two growth stages. Stage I–from the instant when NPs are mixed with homoPEs up to 40 min–is characterized by the formation of aggregates of NPs and homoPEs that progressively increase in size from the D_H of single NPs to 250 nm. The growth rate is ~4.8 nm min^{-1} and the size of the aggregates obtained at the end of stage I is remarkably similar for both mixtures made of PDADMAC and PEI. Stage II, from 40 min to 120 min for NPs + PDADMAC mixture and to 145 min for NPs + PEI mixture, is characterized by a faster growth rate of 22.9 nm min^{-1} for NPs + PDADMAC mixture and 17.5 nm min^{-1} for NPs + PEI mixture. In this stage, the D_H of the aggregates increases from 250 nm to ~1900 nm and then remains stable. No visual phase separation was found in the turbid mixture solution during the following two hours.

For both mixtures, electrostatic interactions were stopped at the end of stage I by addition of salt and synthesized aggregates purified and dispersed in water. Presence of salt during a short period did not trigger disassembling of the aggregates probably because Van der Waals forces and entanglements between polymer chains maintain the structures. TEM images of NPs + PDADMAC (Fig. 1(b, c)) and NPs + PEI (Fig. S9(b, c)) show ~200 nm well-defined spherical aggregates made of densely packed nanoparticles. The polydispersity of these stable colloids is remarkably low, which demonstrates the controllability of the process. Aggregates obtained at the beginning of stage II are pictured in Fig. 1(d) and Fig. S9(d). TEM images illustrate clusters of randomly-packed spherical aggregates formed during the first stage. Fig. 1(e) and Fig. 1(f) (respectively Figs. S9(e) and (f)) are TEM and SEM images of the ~2 μm coral-like aggregates obtained at the end of stage II. Insert images to Fig. 1(e) and Fig. S9(e) present high magnification TEM images revealing internal nanostructures where nanoparticles are densely packed and spherical "seeds" still visible.

The effect of concentration on aggregation is studied by direct mixing of γ-Fe_2O_3-PAA_{2K} NPs dispersions with PDADMAC or PEI solution (mixtures at IP, pH = 7 and at their respective I_s^c) at 0.5 wt.%, 0.05 wt.% and 0.005 wt.%. Fig. 2 displays the time evolutions of the hydrodynamic diameters (D_H) of NPs + PDADMAC mixtures (Fig. 2(a)) and of the NPs + PEI mixtures (Fig. 2(e)).

For both homoPEs and for the three concentrations, a two-stage growth process is observed. Stage I: up to 50 min at 0.005 wt.% and up to 20 min at 0.5 wt.% for NPs + PDADMAC; this was up to 55 min at 0.005 wt.% and up to 30 min at 0.5 wt.% for NPs + PEI. Stage I is shorter and has an increase in growth rates of ~94% with a weight concentration increase of one hundred times. Stage II is characterized by significant increases in the growth rate from 18.1 nm min^{-1}

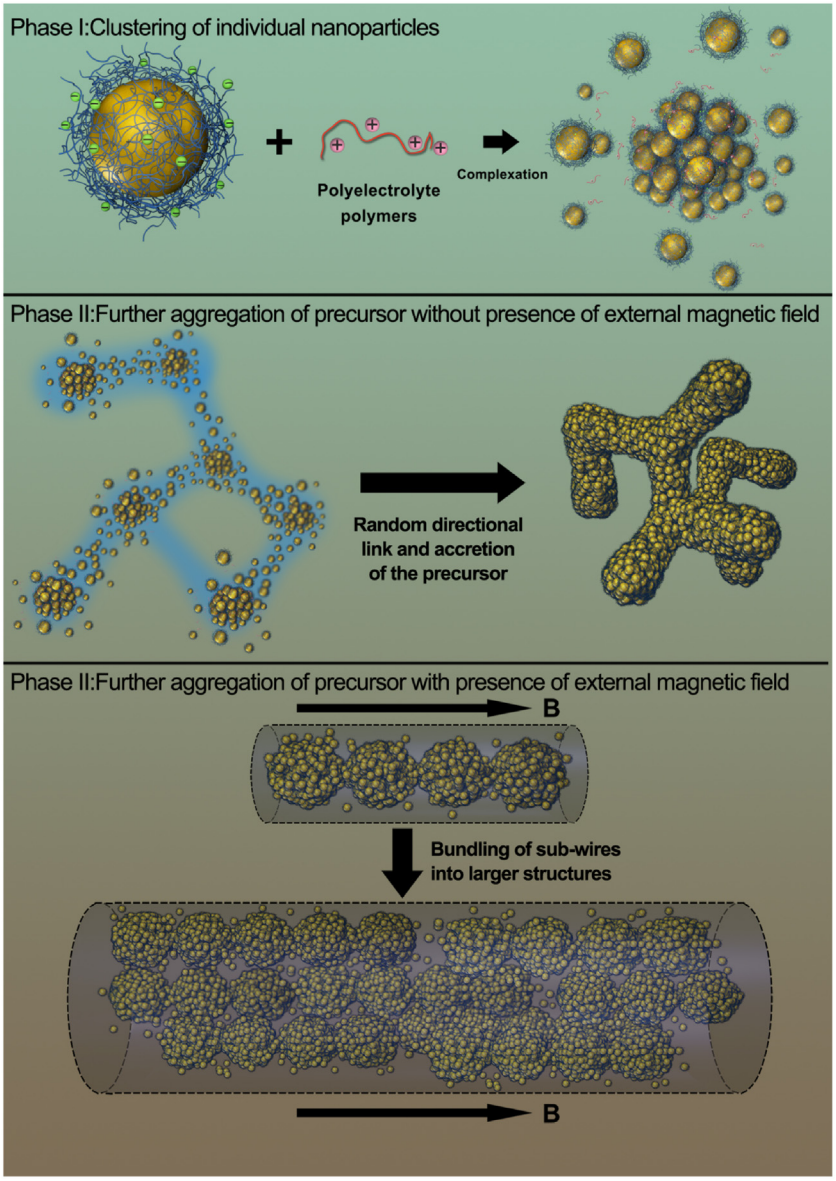

Scheme 2. Schematic representation of growth mechanism of aggregates made by direct mixing of anionic superparamagnetic NPs and cationic homoPEs in dispersion at IP with pH = 7. The direct mixing was performed at the I_s^c with and without the presence of an external magnetic field of 0.3 T.

at 0.005 wt.% to 58.6 nm min^{-1} at 0.5 wt.% for NPs + PDADMAC and from 14.8 nm min^{-1} at 0.005 wt.% to 78.6 nm min^{-1} at 0.5 wt.% for NPs + PEI. Mixtures at 0.5 wt.% finally formed large aggregates whose size is beyond the range of the DLS instrument (>5 μm). The large aggregates precipitate under gravity with the formation of phase separation. At this concentration (0.5 wt.%), SEM images of NPs + PDADMAC (Fig. 2(d)) and of NPs + PEI (Fig. 2(h)) mixtures (obtained at 160 min after direct mixings) show aggregates larger than 10 μm with a dense structure.

At 0.005 wt.%, stage II ends after 135 min for NPs + PDADMAC and 160 min for NPs + PEI with average D_H of 1750 nm and 1600 nm, respectively. As the concentration is decreased from 0.05 wt.% to 0.005 wt.%, the aggregation stopped later as a consequence of the slower growth rate. The aggregates from 0.005 wt.% (Fig. 2(b) and (f)) exhibit similar coral-like architecture as the ones from 0.05 wt.% (Fig. 2(c) and (g)) but with smaller sizes and more expanded structures.

Considering the above data and discussion, it is reasonable to conclude that the growth mechanism of aggregation is initially from "seed" aggregation of individual NPs into 200 nm spherical aggregates (Fig. 1(b, c) and Fig. S9(b, c)). Random directional linkages and accretion of the spherical precursors, as illustrated by Fig. 1(d) and Fig. S9(d) follows. Progressively, clusters aggregate into micron-sized colloids (Fig. 1(e, f), Fig. S9(e, f) and SEM images of Fig. 2). During the entire accretion phenomenon, unreacted individual nanoparticles and polyelectrolyte chains complex with already existing aggregates, acting like a cement to finally give larger and denser nanostructures. The packing density of the 200 nm spherical precursors inside the final aggregates, as well as their overall size, decreases with the initial concentration of NPs and polyelectrolytes. This concentration-dependent accretion process induces a gradient of possible morphologies that range from relatively large and compact "rocks" at high concentration to small but "latticed corals" at low concentration. The first and second panels of Scheme 2 illustrate the two-step growth mechanism.

Under strong driving forces, e.g. electrostatic interaction and/or hydrogen bonding, the key factor controlling the polydispersity and the final size of the colloidal complexes is competition between

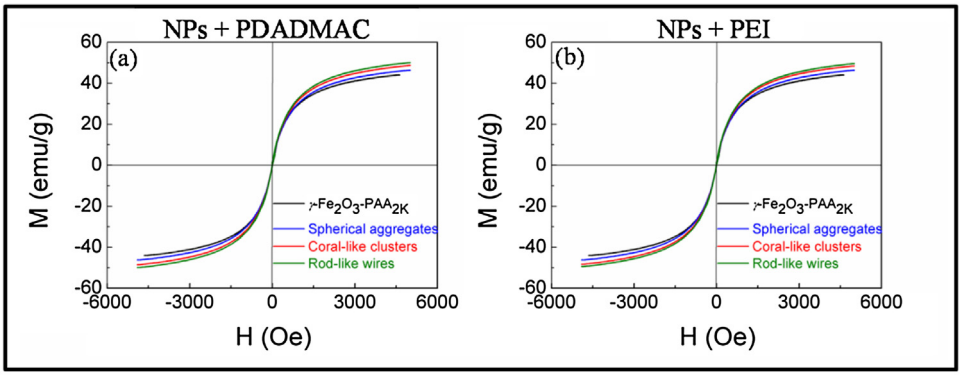

Fig. 3. Magnetic field dependence of the macroscopic magnetization M(H) at 25 °C for γ-Fe_2O_3-PAA_{2K} NPs dispersions (black), for the spherical aggregates obtained at the end of the stage I of a mixture (blue), for the coral-like clusters obtained at the end of the stage II (red) and for the rod-like wires obtained with the presence of external magnetic (green). (a) Results from direct mixings of γ-Fe_2O_3-PAA_{2K} NPs dispersions and PDADMAC solutions at 0.05 wt.%. (b) Results from direct mixings of γ-Fe_2O_3-PAA_{2K} NPs dispersions and PEI solutions at 0.05 wt.%. (For interpretation of the references to colour in this figure legend, the reader is referred to the web version of this article.)

the reaction time T_r of the components and the homogenization time T_h of the mixed solution [53,54]. When the T_r is less than T_h, local concentration inhomogeneity leads to the formation of polydisperse structures. Moreover, the resulting structures are not in thermodynamic equilibrium; thus, their morphology is uncontrollable. This is the case for NPs and homoPEs mixtures at $I_s = 0$ M, where T_r is fast compared with T_h. Thus, the key to controlling the colloidal aggregation is to allow the reaction timescales to be significantly longer than T_h. This is achieved experimentally at I_s^c where the salt screens the electrostatic interactions and greatly reduces the kinetics of the reaction. The T_h remains the same as in the other experiments, and T_r can be extended several orders of magnitude. These results indicate that by choosing appropriate I_s in aqueous medium, spontaneous assembly/aggregation can be effectively moderated by increasing the T_r, and result in controlled colloidal aggregation.

Aggregates produced from direct mixing at an appropriate I_s and concentrations below 0.05 wt.% have good colloidal stability and a regulated size of ~2 μm. However, as a result of the aggregation mechanism, their coral-like form is not controlled. Fig. 3 presents magnetization as a function of the applied magnetic field at 25 °C. The samples include γ-Fe_2O_3-PAA_{2K} NPs, the ~200 nm spherical aggregates obtained at the end of the stage I of a NPs/homoPEs mixture at 0.05 wt.%, the coral-like clusters obtained at the end of the stage II at 0.05 wt.%, and the rod-like wires obtained via an external magnetic field. All the samples exhibit a superparamagnetic behavior with similar magnetization saturation values of ~44 emu g^{-1} for the polymer coated NPs, ~46 emu g^{-1} for the spherical aggregates, ~48 emu. g^{-1} for the coral-like clusters and ~49 emu. g^{-1} for the rod-like wires.

The superparamagnetic behavior of the spherical aggregates obtained at the end of the stage I indicates that the magnetic dipole interactions are not responsible for the clustering observed during stage II. Moreover, these spherical aggregates are stable at high ionic strength. This indicates that the Van der Waals interactions do not drive aggregation at this stage of growth. Thus, clustering is mainly a consequence of electrostatic assembly between the reactive species in the aqueous medium.

At the beginning of stage II, the concentration of the reactive species is lower than the initial values because most of the NPs are bound as spherical aggregates. Consequently the weakened electrostatic interactions facilitate diffusion of the species at long timescales before their interaction. However, when the initial concentration is high, e.g. 0.5 wt.%, the spherical precursors are numerous and close to each other. In this case, the aggregation is not limited by their diffusion and densely packed aggregates are formed (Fig. 2(d) and (h)). Over time, aggregation results in the clustering of bigger and bigger objects. As they progressively cluster, their number per unit volume decreases, and the influence of diffusion in the aggregation process increases. As result, the aggregates obtained at the end of stage II are not spherical but randomly shaped.

When the initial concentration are decreased to 0.05 wt.% and to 0.005 wt.%, local concentration of ~200 nm spherical precursors at the beginning of stage II is sufficiently low such that the diffusion becomes a parameter that can greatly influence the clustering. The coral-like structures observed on SEM (Fig. 2(b), (c), (f) and (g)) originate from the contact of the spherical precursors after a random walk due to Brownian motion. The diffusion limits are as strong as the concentration is low. This results in increasingly expanded coral-like structures and an increasingly random morphology. The sensitivity of the aggregation mechanism to concentration supports the hypothesis that diffusion is the key factor influencing the morphology of the colloidal aggregates. This diffusion-limited aggregation mechanism is expected to be independent of the chemical nature of the oppositely charged species.

In this section, the direct mixing protocols of NPs and homoPEs were repeated in the presence of an external 0.3 T magnetic field. Fig. 4 shows DLS and microscopy studies of a NPs + PDADMAC mixture at 0.05 wt.%. The results obtained from the NPs + PEI mixtures at 0.05 wt.% are presented in ESI–3. The DLS experiments show that direct mixing in a magnetic field for both PDADMAC and PEI have two growth stages (Fig. 4(a) and Fig. S10(a)). The first stage is the same as the case without external magnetic field, that is, assembly from single particles to $D_H \sim 250$ nm aggregates within 40 min and at the same growth rate. These ~200 nm spherical aggregates are formed by the dense packing of single NPs (Fig. 4(b), (c) and Fig. S10(b), (c)). In the second stage, measured D_H increase quickly and reach the resolution of DLS after 20 min. Aggregates obtained at the beginning of stage II (40 min) are depicted in TEM images of Fig. 4(d) and Fig. S10(d). It is observed that, with the presence of external magnetic field during assembly, the spherical aggregates formed during the first stage are packed together in clusters with a tendency to be aligned. 60 min after direct mixing, well-defined and regular ~2 μm cylindrical aggregates are obtained, as shown by TEM images of Fig. 4(e) and Fig. S10(e). Their diameter of 200 nm is consistent with the diameter of the previous spherical clusters. TEM images of Fig. 4(f) and Fig. S10(f) illustrate the structure of the larger rod-like aggregates obtained after 120 min of reaction. These aggregates are bundles of assembled multiple sub-wires observed at earlier stage (Fig. 4(e) and Fig. S10(e)). High magnification TEM image presented in the insert to Fig. 4(f) reveals the cylindrical structure of sub-wires and their nanostructure made of densely packed nanoparticles. SEM images of Fig. 4(g) and Fig. S10(g) are

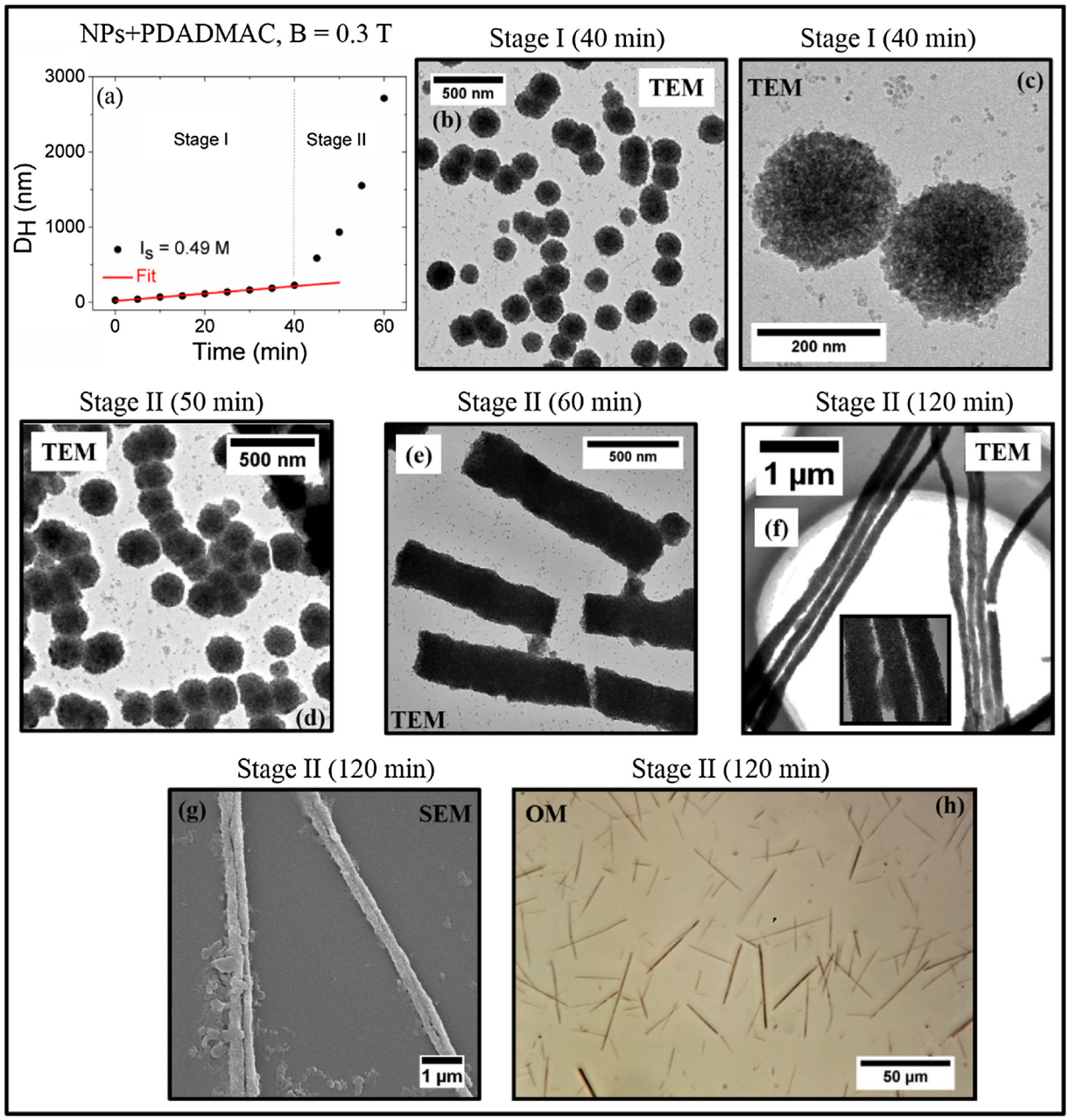

Fig. 4. (a) D_H versus time of direct mixings of γ-Fe_2O_3-PAA_{2K} NPs dispersions and PDADMAC solutions at 0.05 wt.% and at I_s^c with the presence of 0.3 T magnetic field. A two stages growth mechanism is observed. Stage I: "seed" clustering into D_H ~250 nm spherical aggregates. Stage II: alignment of the spherical clusters into sub-wires and their assembly into larger wires. (b) and (c) TEM image of the spherical aggregates obtained at the end of stage I (40 min). (d) TEM image, obtained at the beginning of stage II (50 min), of quasi one-dimensional clusters made of spherical aggregates. (e) TEM image of cylindrical aggregates obtained during stage II (60 min). (f) TEM, (g) SEM, and (h) optical microscopy images of large rod-like aggregates obtained at the end of stage II (120 min).

representative of the straight rod-like aggregates obtained 120 min after mixing. They confirm the bounded structures consisting of smaller sub-wires. Fig. 4(h) and Fig. S10(h) are optical transmission microscopy (OM) images of NPs + PDADMAC and NPs + PEI samples, respectively, 120 min after direct mixing. Straight rod-like aggregates with random orientations and typical lengths between 10 μm and 50 μm are observed. A series of OM images were quantitatively analyzed to retrieve the length distribution (ESI–4). The median length of NP/PDADMAC and NP/PEI rod-like aggregates is 20 ± 3 μm and 17 ± 1 μm, respectively. The polydispersity of both is 0.5. If a magnet is brought near the sample, the wires reoriented spontaneously and followed the magnetic field lines. Coupling between the wires and the external field originates from the superparamagnetic properties exhibited by the elongated structures [38]. The similar lengths, widths and microstructures of NP/PDADMAC and NP/PEI wires again highlight the indifference of the polymer type for this assembly method.

The growth mechanism of magnetic wires made of anionic superparamagnetic NPs and homoPEs can be described as follows. First, "seed" assembly of individual nanoparticles into ~200 nm spherical aggregates. Second, alignment of the precursor aggregates into one-dimensional clusters (sub-wires) induced by their magnetic dipolar interactions. Third, bundling of the sub-wires into larger structures. During this step, magnetic dipolar interactions bring sub-wires side to side whereas electrostatic interaction and Van der Waals forces sticks them together. The first and third pan-

els of Scheme 2 illustrate the growth mechanism of the wires under external magnetic fields. Assumption of this mechanism presented in previous study [40] has now been evidenced by the "time frame" images of Fig. 4 rendered possible by the slowed-down interaction process. A dynamic representation of the discovered growth mechanism is proposed in an animation video in the supplement.

4. Conclusions

A simple, efficient and general approach for moderating the assembly driven by electrostatic interaction between colloidal NPs and widespread homopolyelectrolytes is established. The oppositely charged species are directly mixed in aqueous media at an appropriate I_s where the electrostatic interaction can be nearly screened with respect to the extension of reaction time. The growth mechanisms of the resulting aggregates are rationalized first as "seed" growth of spherical precursors (250 nm) from single NPs and second followed by a random link and accretion of the precursors into coral-like clusters. In the presence of an external magnetic field, the mechanism is conclude as first, same "seed" growth of 200 nm spherical clusters. Second, alignment of the 200 nm spherical clusters into one-dimensional sub-wires induced by magnetic dipolar interactions. Third, assembly of the sub-wires into "bundled" larger structures. Using this approach, direct mixing of oppositely charged species in solution can generate both spherical clusters and cylindrical aggregates with controlled size and morphology with minimum restriction of specific assembly devices and nature of the polycations.

Notes

The authors declare no competing financial interest.

Acknowledgements

This research was supported by Sichuan Province Education Department Innovation Team Foundation (16zd1104); Sichuan Province Science Foundation for Young Scientists (No. 15zs2111); Open Project of the Key Laboratory of Neutron Physics and Institute of Nuclear Physics and Chemistry, China Academy of Engineering Physics (No. 2014BB06) and by Research Funding of Southwest University of Science and Technology (Nos. 13zx7135, 14zx7118, 14tdfk08, 15zx7101, 15zx7108, 15yyhk14 and 15zxt101).

Appendix A. Supplementary data

Supplementary data associated with this article can be found, in the online version, at http://dx.doi.org/10.1016/j.colsurfa.2016.11.049.

References

[1] A.M. Kalsin, M. Fialkowski, M. Paszewski, S.K. Smoukov, K.J.M. Bishop, B.A. Grzybowski, Electrostatic self-assembly of binary nanoparticle crystals with a diamond-like lattice, Science 312 (2006) 420–424.
[2] Z. Tang, Z. Zhang, Y. Wang, S.C. Glotzer, N.A. Kotov, Self-assembly of CdTe nanocrystals into free-floating sheets, Science 314 (2006) 274–278.
[3] M.E. Leunissen, C.G. Christova, A.-P. Hynninen, C.P. Royall, A.I. Campbell, A. Imhof, M. Dijkstra, R. van Roij, A. van Blaaderen, Ionic colloidal crystals of oppositely charged particles, Nature 437 (2005) 235–240.
[4] E.V. Shevchenko, D.V. Talapin, N.A. Kotov, S. O'Brien, C.B. Murray, Structural diversity in binary nanoparticle superlattices, Nature 439 (2006) 55–59.
[5] S.Y. Park, A.K.R. Lytton-Jean, B. Lee, S. Weigand, G.C. Schatz, C.A. Mirkin, DNA-programmable nanoparticle crystallization, Nature 451 (2008) 553–556.
[6] R. Klajn, K.J.M. Bishop, M. Fialkowski, M. Paszewski, C.J. Campbell, T.P. Gray, B.A. Grzybowski, Plastic and moldable metals by self-assembly of sticky nanoparticle aggregates, Science 316 (2007) 261–264.
[7] M.M. Maye, J. Luo, I.I.S. Lim, L. Han, N.N. Kariuki, D. Rabinovich, Liu, C.-J. Zhong, Size-controlled assembly of gold nanoparticles induced by a tridentate thioether ligand, J. Am. Chem. Soc. 125 (2003) 9906–9907.
[8] Z. Mao, H. Xu, D. Wang, Molecular mimetic self-assembly of colloidal particles, Adv. Funct. Mater. 20 (2010) 1053–1074.
[9] Z. Nie, A. Petukhova, E. Kumacheva, Properties and emerging applications of self-assembled structures made from inorganic nanoparticles, Nat. Nanotechnol. 5 (2010) 15–25.
[10] G. Gopalakrishnan, C. Danelon, P. Izewska, M. Prummer, P.-Y. Bolinger, I. Geissbühler, D. Demurtas, J. Dubochet, H. Vogel, Multifunctional lipid/quantum dot hybrid nanocontainers for controlled targeting of live cells, Angew. Chem. Int. Ed. 45 (2006) 5478–5483.
[11] H. Jia, S. Titmuss, Polymer-functionalized nanoparticles: from stealth viruses to biocompatible quantum dots, Nanomedicine 4 (2009) 951–966.
[12] R. Elghanian, J.J. Storhoff, R.C. Mucic, R.L. Letsinger, C.A. Mirkin, Selective colorimetric detection of polynucleotides based on the distance-dependent optical properties of gold nanoparticles, Science 277 (1997) 1078–1081.
[13] J.-S. Lee, P.A. Ulmann, M.S. Han, C.A. Mirkin, A DNA-gold nanoparticle-based colorimetric competition assay for the detection of cysteine, Nano Lett. 8 (2008) 529–533.
[14] J. Lee, P. Hernandez, J. Lee, A.O. Govorov, N.A. Kotov, Exciton-plasmon interactions in molecular spring assemblies of nanowires and wavelength-based protein detection, Nat. Mater. 6 (2007) 291–295.
[15] E. Ozbay, Plasmonics: merging photonics and electronics at nanoscale dimensions, Science 311 (2006) 189–193.
[16] M.P. Genovese, I.V. Lightcap, P.V. Kamat, Sun-believable solar paint. a transformative one-step approach for designing nanocrystalline solar cells, ACS Nano 6 (2012) 865–872.
[17] P.K. Santra, P.V. Kamat, Tandem-layered quantum dot solar cells: tuning the photovoltaic response with luminescent ternary cadmium chalcogenides, J. Am. Chem. Soc. 135 (2013) 877–885.
[18] S.A. Maier, P.G. Kik, H.A. Atwater, S. Meltzer, E. Harel, B.E. Koel, A.A.G. Requicha, Local detection of electromagnetic energy transport below the diffraction limit in metal nanoparticle plasmon waveguides, Nat. Mater. 2 (2003) 229–232.
[19] C.-J. Wang, L. Huang, B.A. Parviz, L.Y. Lin, Subdiffraction photon guidance by quantum-dot cascades, Nano Lett. 6 (2006) 2549–2553.
[20] T. Yatsui, Y. Ryu, T. Morishima, W. Nomura, T. Kawazoe, T. Yonezawa, M. Washizu, H. Fujita, M. Ohtsu, Self-assembly method of linearly aligning ZnO quantum dots for a nanophotonic signal transmission device, Appl. Phys. Lett 96 (2010) 133106.
[21] G. Kawamura, Y. Yang, M. Nogami, Facile assembling of gold nanorods with large aspect ratio and their surface-enhanced Raman scattering properties, Appl. Phys. Lett. 90 (2007) 261908.
[22] J.N. Anker, W.P. Hall, O. Lyandres, N.C. Shah, J. Zhao, R.P. Van Duyne, Biosensing with plasmonic nanosensors, Nat. Mater. 7 (2008) 442–453.
[23] K.K. Caswell, J.N. Wilson, U.H.F. Bunz, C.J. Murphy, Preferential end-to-end assembly of gold nanorods by biotin-streptavidin connectors, J. Am. Chem. Soc. 125 (2003) 13914–13915.
[24] Z. Nie, D. Fava, E. Kumacheva, S. Zou, G.C. Walker, M. Rubinstein, Self-assembly of metal-polymer analogues of amphiphilic triblock copolymers, Nat. Mater. 6 (2007) 609–614.
[25] D. Zerrouki, J. Baudry, D. Pine, P. Chaikin, J. Bibette, Chiral colloidal clusters, Nature 455 (2008) 380–382.
[26] M.E. Leunissen, R. Dreyfus, F.C. Cheong, D.G. Grier, R. Sha, N.C. Seeman, P.M. Chaikin, Switchable self-protected attractions in DNA-functionalized colloids, Nat. Mater. 8 (2009) 590–595.
[27] Nie, D. Fava, M. Rubinstein, E. Kumacheva, Supramolecular assembly of gold nanorods end-Terminated with polymer pom-poms: Effect of pom-pom structure on the association modes, J. Am. Chem. Soc. 130 (2008) 3683–3689.
[28] K. Liu, Z. Nie, N. Zhao, W. Li, M. Rubinstein, E. Kumacheva, Step-growth polymerization of inorganic nanoparticles, Science 329 (2010) 197–200.
[29] A.B. Davila-Ibanez, N.J. Buurma, V. Salgueirino, Assessment of DNA complexation onto polyelectrolyte-coated magnetic silica nanoparticles, Nanoscale 5 (2013) 4797–4807.
[30] D.A. Walker, B. Kowalczyk, M.O. de la Cruz, B.A. Grzybowski, Electrostatics at the nanoscale, Nanoscale 3 (2011) 1316–1344.
[31] J.P. Chapel, J.F. Berret, Versatile electrostatic assembly of nanoparticles and polyelectrolytes: coating, clustering and layer-by-layer processes, Curr. Opin. Colloid Interface Sci. 17 (2012) 97–105.
[32] M. Antonietti, J. Conrad, Synthesis of very highly ordered liquid crystalline phases by complex formation of polyacrylic acid with cationic surfactants, Angew. Chem. Int. Ed. Engl. 33 (1994) 1869–1870.
[33] S. Zhou, F. Yeh, C. Burger, B. Chu, Formation and transition of highly ordered structures of polyelectrolyte-surfactant complexes, J. Phys. Chem. B 103 (1999) 2107–2112.
[34] J.-F. Berret, Stoichiometry of electrostatic complexes determined by light scattering, Macromolecules 40 (2007) 4260–4266.
[35] Y. Wang, K. Kimura, Q. Huang, P.L. Dubin, W. Jaeger, Effects of salt on polyelectrolyte-micelle coacervation, Macromolecules 32 (1999) 7128–7134.
[36] Y. Wang, K. Kimura, P.L. Dubin, W. Jaeger, Polyelectrolyte-micelle coacervation: effects of micelle surface charge density, polymer molecular weight, and Polymer/Surfactant ratio, Macromolecules 33 (2000) 3324–3331.
[37] M. Yan, J. Fresnais, S. Sekar, J.P. Chapel, J.F. Berret, Magnetic nanowires generated via the waterborne desalting transition pathway, ACS Appl. Mater. Interfaces 3 (2011) 1049–1054.
[38] J. Fresnais, J.-F. Berret, B. Frka-Petesic, O. Sandre, R. Perzynski, Electrostatic co-assembly of iron oxide nanoparticles and polymers: towards the

generation of highly persistent superparamagnetic nanorods, Adv. Mater. 20 (2008) 3877–3881.
[39] M. Yan, L. Qu, J. Fan, Y. Ren, Electrostatic complexation of polyelectrolyte and magnetic nanoparticles: from wild clustering to controllable magnetic wires, Nanoscale Res. Lett. 9 (2014) 1–14.
[40] M. Yan, J. Fresnais, J.F. Berret, Growth mechanism of nanostructured superparamagnetic rods obtained by electrostatic co-assembly, Soft Matter 6 (2010) 1997–2005.
[41] K.E.V. Holde, Chromatin, Springer-Verlag, New York, 1989.
[42] R. Massart, E. Dubois, V. Cabuil, E. Hasmonay, Preparation and properties of monodisperse magnetic fluids, J. Magn. Magn. Mater. 149 (1995) 1–5.
[43] S. Lefebure, E. Dubois, V. Cabuil, S. Neveu, R. Massart, Monodisperse magnetic nanoparticles: preparation and dispersion in water and oils, J. Mater. Res. 13 (1998) 2975–2981.
[44] I.T. Lucas, S. Durand-Vidal, E. Dubois, J. Chevalet, P. Turq, Surface charge density of maghemite nanoparticles: role of electrostatics in the proton exchange, J. Phys. Chem. C 111 (2007) 18568–18576.
[45] A. Sehgal, Y. Lalatonne, J.-F. Berret, M. Morvan, Precipitation-redispersion of cerium oxide nanoparticles with poly(acrylic acid): toward stable dispersions, Langmuir 21 (2005) 9359–9364.
[46] J. Tang, M. Myers, K.A. Bosnick, L.E. Brus, Magnetite Fe3O4 nanocrystals: spectroscopic observation of aqueous oxidation kinetics, J. Phys. Chem. B 107 (2003) 7501–7506.
[47] J. Fresnais, M. Yan, J. Courtois, T. Bostelmann, A. Bee, J.F. Berret, Poly(acrylic acid)-coated iron oxide nanoparticles: quantitative evaluation of the coating properties and applications for the removal of a pollutant dye, J. Colloid Interface Sci. 395 (2013) 24–30.
[48] M. Ballauff, O. Borisov, Polyelectrolyte brushes, Curr. Opin. Colloid Interface Sci. 11 (2006) 316–323.
[49] J.N. Israelachvili, Intermolecular and Surfaces Forces, 2nd ed., Academic Press, New York, 1992.
[50] P. Lindner, T. Zemb, Neutrons, X-rays and Light: Scattering Methods Applied to Soft Condensed Matter, Elsevier, Amsterdam, 2002.
[51] A. Horovitz, L. Serrano, B. Avron, M. Bycroft, A.R. Fersht, Strength and co-operativity of contributions of surface salt bridges to protein stability, J. Mol. Biol. 216 (1990) 1031–1044.
[52] E. Kokufuta, H. Suzuki, R. Yoshida, K. Yamada, M. Hirata, F. Kaneko, Role of hydrogen bonding and hydrophobic interaction in the volume collapse of a poly(ethylenimine) gel, Langmuir 14 (1998) 788–795.
[53] L. Qi, J. Fresnais, J.-F. Berret, J.-C. Castaing, F. Destremaut, J.-B. Salmon, F. Cousin, J.-P. Chapel, Influence of the formulation process in electrostatic assembly of nanoparticles and macromolecules in aqueous solution: the interaction pathway, J. Phys. Chem. C 114 (2010) 16373–16381.
[54] L. Qi, J. Fresnais, J.-F. Berret, J.-C. Castaing, I. Grillo, J.-P. Chapel, Influence of the formulation process in electrostatic assembly of nanoparticles and macromolecules in aqueous solution: the mixing pathway, J. Phys. Chem. C 114 (2010) 12870–12877.